

Characterization of Radiation Exposure at Aviation Flight Altitudes Using the Nowcast of Aerospace Ionizing Radiation System (NAIRAS)

Daniel Phoenix¹, Christopher J. Mertens¹, Guillaume Gronoff², and Kent Tobiska³

¹NASA Langley Research Center

²Nasa Langley Research Center

³Space Weather Division, Space Environment Technologies

January 23, 2024

Abstract

Exposure to ionizing radiation from galactic cosmic rays (GCR) and solar energetic particles (SEP) at aircraft flight altitudes can have an adverse effect on human health. Although airline crews are classified as radiation workers by the International Commission on Radiological Protection (ICRP), in most countries, their level of exposure is unquantified and undocumented throughout the duration of their career. As such, there is a need to assess pilot ionizing radiation exposure. The Nowcast of Aerospace Ionizing Radiation System (NAIRAS), a real-time, global, physics-based model is used to assess such exposure. The Automated Radiation Measurements for Aerospace Safety (ARMAS) measurement dataset consists of high latitude, high altitude, and long-duration aircraft flights between 2013-2023. Here, we characterize radiation exposure at aviation flight altitudes using the NAIRAS model and compare with 45 flight trajectories from the recent ARMAS flight measurement inventory.

Hosted file

985152_0_art_file_11798651_s7jt28.docx available at <https://authorea.com/users/593079/articles/705561-characterization-of-radiation-exposure-at-aviation-flight-altitudes-using-the-nowcast-of-aerospace-ionizing-radiation-system-nairas>

Characterization of Radiation Exposure at Aviation Flight Altitudes Using the Nowcast of Aerospace Ionizing Radiation System (NAIRAS)

Daniel B. Phoenix^{1,2,3}, Chris J. Mertens³, Guillaume P. Gronoff^{2,3}, and Kent Tobiska⁴

¹. Analytical Mechanics Associates, Hampton, VA, USA

². Science Systems and Applications, Inc., Hampton, VA, USA

³. NASA Langley Research Center, Hampton, VA, USA

⁴. Space Environment Technologies, Pacific Palisades, CA, USA

Corresponding author: Daniel B. Phoenix (daniel.b.phoenix@nasa.gov)

Key Points

- The ARMAS dosimeter flew on board and measured dose rates for 39 corporate and 6 research flights between August 2022 and March 2023.
- The NAIRAS Run on Request model was run for each flight and produces dose estimates in agreement with the ARMAS dosimeter.
- Results show that airline crew radiation exposure does not exceed the ICRP standard but could invoke individual radiation monitoring.

47 Abstract

48 Exposure to ionizing radiation from galactic cosmic rays (GCR) and solar energetic particles
49 (SEP) at aircraft flight altitudes can have an adverse effect on human health. Although airline
50 crews are classified as radiation workers by the *International Commission on Radiological*
51 *Protection (ICRP)*, in most countries, their level of exposure is unquantified and undocumented
52 throughout the duration of their career. As such, there is a need to assess pilot ionizing radiation
53 exposure. The Nowcast of Aerospace Ionizing RADIation System (NAIRAS), a real-time, global,
54 physics-based model is used to assess such exposure. The Automated Radiation Measurements
55 for Aerospace Safety (ARMAS) measurement dataset consists of high latitude, high altitude, and
56 long-duration aircraft flights between 2013-2023. Here, we characterize radiation exposure at
57 aviation flight altitudes using the NAIRAS model and compare with 45 flight trajectories from
58 the recent ARMAS flight measurement inventory.

60 Plain Language Summary

61 The Nowcast of Aerospace Ionizing RADIation System (NAIRAS) model and the Automated
62 Radiation Measurements for Aerospace Safety (ARMAS) dosimeter were used to estimate
63 radiation exposure for airline crews. Radiation dose rates were measured and calculated for 45
64 fairly representative flights between August 2022 and March 2023. Model results showed good
65 agreement with the dosimeter and suggest that although airline crews on these flights were not
66 exposed to radiation at levels exceeding the international standard, they would be candidates for
67 individual radiation monitoring.

69 1 Introduction

70 Aircraft flying at typical commercial and corporate airline altitudes in the upper troposphere and
71 lower stratosphere are constantly exposed to extraterrestrial, high-energy charged particles and
72 secondary neutrons. Energetic particles at these altitudes can affect aircraft microelectronic
73 systems and the health of airline crews and passengers (Wilson, 2000; IEC, 2006). This type of
74 particle radiation comes from two main sources: (1) the ever-present galactic cosmic radiation
75 (GCR), which originates from outside our solar system, and (2) solar energetic particles (SEP),
76 which are associated with eruptions on the Sun's surface and typically only last for several hours
77 to days (Wilson et al., 1991; Gopalswamy et al., 2003).

78
79 Due to this exposure, airline crews are classified as radiation workers by the *International*
80 *Commission on Radiological Protection (ICRP)* (1991). In several recent studies, it was found
81 that airline crews in the United States have received the highest average effective dose among all
82 radiation workers surveyed (NCRP, 2009). Additionally, a study of Air Canada pilots showed
83 that most pilots were exposed to over 1 mSv, with the majority receiving between 3 and 5 mSv
84 (Bennett et al., 2013). An exposure of 1 mSv is enough to warrant an individual exposure
85 assessment in some countries (Linborg and Nikjoo, 2011). Furthermore, the flights on high-
86 latitude or intercontinental routes are at risk of exceeding the maximum public and prenatal
87 exposure during a single SEP event or through several (~5-10) round-trip, high-latitude flights
88 from GCR exposure (AMS, 2007; Copeland et al., 2008; Dyer et al., 2009; Mertens et al., 2012).
89 Importantly, while some countries do monitor airline crew exposure, many countries do not,
90 making airline crews the only occupational group to be exposed to both unquantified and
91 undocumented levels of radiation over their career. As such, there is a need to develop tools to

92 extend the current scientific knowledge of the atmospheric ionizing radiation field for the benefit
93 of decision making and planning within the aviation community.

94
95 Currently, there are a number of models for assessing radiation exposure available to the aviation
96 community. The following models have been recently compared: the CARI-7A (Civil
97 Aeromedical Research Institute) model (Copeland et al., 2010; Copeland, 2017), which is used
98 by the Federal Aviation Administration, the PANDOCA (Professional Aviation Dose Calculator)
99 model (Matthiä et al., 2013, 2014), which is used by the German Aerospace Center, and the
100 Nowcast of Aerospace Ionizing RAdiation System (NAIRAS, Mertens et al., 2023b). Previous
101 efforts to evaluate model calculated radiation doses at aviation cruise altitudes have been limited
102 by the availability of reliable high-quality dose rate measurements, particularly for the severe,
103 high dose radiation events. Nevertheless, model evaluation studies have been performed using
104 measurements of the omnipresent background radiation environment from galactic cosmic
105 radiation (GCR). In Meier et al. (2018), the CARI-7A, PANDOCA, and NAIRAS models were
106 evaluated using observations from two flight missions: the Comparison of Airborne RAdiation
107 Measuring Equipment for implementation of Legal requirements (CARMEL) campaign
108 (Wissmann et al., 2010) and the COmparison of COsmic Radiation Detectors (CONCORD)
109 campaign (Meier et al., 2016). The intercomparison showed that all three models were within
110 20% of the measurements.

111
112 Recent improvements in NAIRAS necessitate an updated evaluation of the model's performance.
113 Additionally, a NASA award was granted to have the ARMAS dosimeter fly on Raytheon
114 corporate flights from August 2022 to April 2023. This new dataset provides an excellent
115 opportunity to (1) evaluate dose rates representative of typical commercial/corporate aircraft
116 routes, (2) evaluate new NAIRAS dose rate calculations for the flight trajectories and compare
117 with ARMAS dosimeter measurements, and (3) compare the dose rate calculations from the
118 previous version of NAIRAS (version 2.0) and the latest version of the model (version 3.0).

119 120 **2 NAIRAS Model Description**

121 The NAIRAS model is a real-time, global, physics-based model developed to calculate radiation
122 exposure to airline crews from both galactic cosmic radiation and solar radiation. The NAIRAS
123 model has been documented previously (Mertens et al., 2010, 2012, 2013). The latest version is
124 described in Mertens et al. (2023a, 2023b, 2023c) and includes several updates, particularly the
125 expansion of the GCR composition, multi-directional atmospheric transport, an improved SEP
126 spectral fitting algorithm, and the inclusion of terrestrial trapped protons (TRP). Here, we
127 summarize the key features of the latest version of the model.

128
129 The GCR composition in the H-BON10 model was expanded to calculate LET spectra out to 100
130 MeV-cm²/mg. Previously, the highest charge and heaviest nuclear isotope in the version of the
131 H-BON10 model was nickel ($Z = 28$, $A = 58$). The new version of NAIRAS has extended the
132 composition of the H-BON10 model to include ultra-heavy GCR nuclear isotopes, with the
133 highest charge and heaviest isotope being uranium ($Z = 92$, $A = 238$).

134
135 To account for the expanded GCR composition, 116 coupled transport equations along each ray
136 direction are required. In the previous version of NAIRAS, the GCR and SEP differential flux at
137 the top of the boundary of the neutral atmosphere was approximated by a projection of a

138 directionally isotropic source along the vertical direction. Recent measurements during the
139 NASA Radiation Dosimetry Experiment (RAD-X) showed that transport along a single direction
140 is insufficient at predicting dosimetric quantities at high-altitudes above commercial aviation
141 cruise altitudes (Norman et al., 2016). Thus, the atmospheric transport in NAIRAS version 3.0
142 was updated to include multi-directional transport through the atmosphere. In addition to GCR
143 and SEP sources of radiation, the new version of NAIRAS now also includes terrestrial trapped
144 protons (TRP). The GEOFFB trapped proton belt model was integrated into NAIRAS version
145 3.0 to extend the model domain from the atmospheric ionizing radiation environment to the
146 geospace radiation environment (Badavi et al., 2011).

147
148 A new proton spectral fitting code was developed in NAIRAS version 3.0 that allows the option
149 to fit a SEP proton spectrum to either the differential GOES proton flux channels or the integral
150 proton flux channels. SEP spectral fitting to the GOES differential proton flux channels has been
151 proven to be problematic during the onset of SEP events and during weak-to-moderate events.
152 The new option to infer the SEP spectrum using GOES integral proton flux channels has enabled
153 a spectrum to be obtained that is consistent with the GOES differential proton channels using a
154 method that is robust against numerical instability and free from erroneous, non-physical fits (see
155 Mertens et al., 2023a, Figure 4).

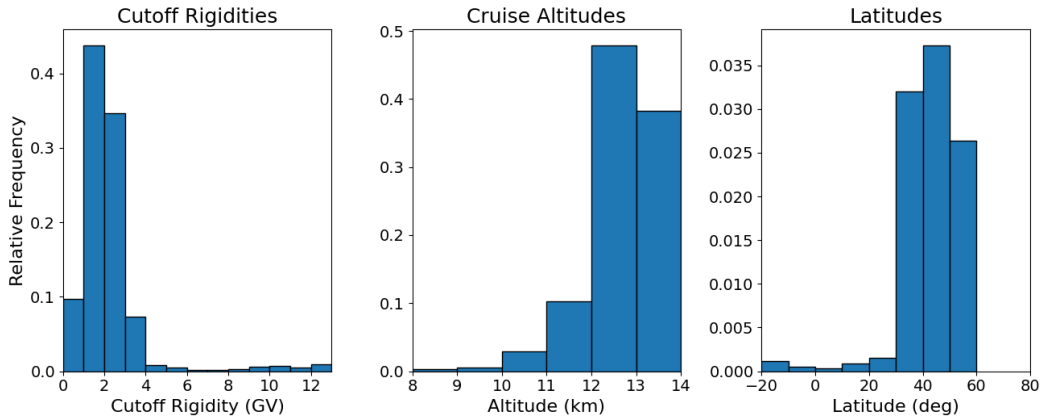
156
157 Transmission of GCR and SEP ions through the geomagnetic field has been improved to capture
158 additional complexities by scaling the numerically-determined vertical cutoff rigidity to other
159 arrival directions. The cutoff rigidity model now also includes an option to use the T89
160 magnetospheric field model (Tsyganenko, 1989), which only needs the Kp-index as an input
161 quantity to calculate the dynamical response to solar-geomagnetic variability. Although the T89
162 model does not capture the magnetospheric response to geomagnetic variability as well as the
163 TS05 model (Tsyganenko and Sitnov, 2005), it does allow for historical solar-geomagnetic storm
164 events to be analyzed prior to 1995.

165
166 **3 ARMAS Flight System**
167 The ARMAS Flight Module (ARMAS FM) unit consists of two components: a flight instrument
168 that measures the real-time radiation total ionizing dose (TID) environment on the aircraft and a
169 calibrated data stream from the aircraft to the ground (Tobiska et al., 2016) using the ARMAS
170 v10.41 and v10.42 data processing systems. The ARMAS system uses a Teledyne micro
171 dosimeter (uDOS001), which directly measures TID absorbed by an internal silicon test mass.
172 The micro dosimeter measures energy absorbed from heavy ions, alphas, protons, neutrons,
173 electrons, and gamma rays, providing an accurate measurement of absorbed dose in silicon. As
174 such, the fundamental quantity measured by the ARMAS dosimeter is the absorbed dose in
175 silicon. All other ARMAS dose quantities are derived by empirical scale factors (Tobiska et al.,
176 2016).

177
178 The dosimeter operates in a wide range of input power voltages that are >13V DC. The
179 accumulated dose resolution is 0.14 μGy and is capable of making measurements in excess of 1
180 kGy. The instrument is typically operated in an aircraft cabin (temperature range 15° C to 25° C),
181 which is well within its acceptable operating range (-30° C to +40° C).

182
183 **4 Description of the Flights**

184 Between August 2022 and April 2023, the ARMAS FM 07008 unit was flown on 45 flights, 39
 185 on Raytheon corporate flights and 6 on NASA Langley Research Center (LaRC) airborne
 186 science research flights. The majority of these flights occurred in the Northern Hemisphere
 187 middle latitudes ($30^{\circ} - 50^{\circ} \text{ N}$), particularly in the United States (Figure 1). About 30% of the
 188 flights were in Europe or transatlantic between Europe and the United States. Only one flight
 189 occurred at low latitudes ($< 30^{\circ} \text{ N}$) and crossed the equator.
 190



191
 192 **Figure 1.** Summary of the cutoff rigidities, cruise altitudes, and latitudes of the Raytheon flights.

193
 194 Additionally, the ARMAS dosimeter collected data on six flights in March 2023 on NASA
 195 LaRC research aircraft (Figure 2) during a science mission in Norway. These six flights all
 196 occurred at high latitude (generally above 60° N) and low cutoff rigidity (generally less than 1
 197 GV) and typically had a cruise altitude of 11-13 km.

198
 199 Overall, considering all 45 flights, the cutoff rigidities at cruise altitude ranged from 1-3 GV
 200 while the cross-equator flight had a mean cutoff rigidity of 10 GV (Fig. 1). The mean cutoff
 201 rigidity of all 45 flights was 2.26 GV. The cruise altitude ranged from 11 – 14 km, with a mean
 202 cruise altitude of 12.5 km for all flights.

203
 204 Flight trajectory information used to run NAIRAS in Run on Request mode was obtained and
 205 processed using FlightAware, with aircraft altitudes provided in barometric altitude coordinates.
 206 This coordinate system is required for running NAIRAS. The use of GPS altitude coordinates
 207 can result in dose rate errors of 50%.

208
 209

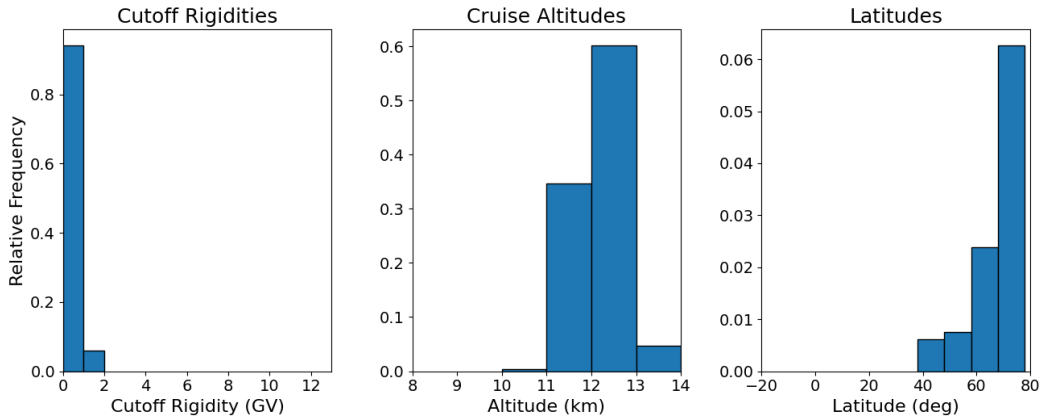


Figure 2. As in Figure 1, but for the six NASA LaRC research flights in Norway.

210
211
212
213

5 Results

5.1 Summary of ARMAS Dose Rates

214
215
216
217
218
219
220
221
222
223
224
225
226
227
228
229
230
231

The collection of Raytheon flights presented in this study are representative of the airline routes that a corporate airline crew would fly. Using the ARMAS dosimeter measurements, we can obtain an accurate estimate of the typical dose rates these airline crews are exposed to. Due to the characteristics of the ARMAS unit, we consider a few constraints on our dataset. First, we only consider measurements that occurred above 8 km in altitude, as it has been demonstrated that the radiation dose is too low below 8 km to achieve good noise statistics in the ARMAS measurements (Tobiska et al., 2016). For a similar reason, we only consider data taken at aircraft cruising altitude because aircraft ascending or descending too quickly will result in a degraded spatial resolution of the measured data. Since the uncertainty in the ARMAS dosimeter has been demonstrated to be 24% (Tobiska et al., 2016), we discard any cruise altitude segments with an average uncertainty in the ARMAS measured absorbed dose rate in silicon of 24% or greater. We also consider other sources of uncertainty such as the analog to digital conversion and the random variation from GCRs. Lastly, to assess how dose rates vary with cutoff rigidity and latitude, we take the average dose rate over cruise durations of at least 30 minutes but no more than 2 hours.

232
233
234
235
236
237
238
239
240
241
242
243
244

Using these criteria, ARMAS dose rates for a typical corporate airline crew are calculated and summarized for all cutoff rigidities in Table 1. The median absorbed dose rate in silicon and tissue were 2.8 and 4.2 $\mu\text{Gy/h}$, respectively, the median dose equivalent rate was 8.6 $\mu\text{Sv/h}$, the median ambient dose equivalent rate was 13.3 $\mu\text{Sv/h}$, and the median effective dose rate was 17.8 $\mu\text{Sv/h}$. Therefore, for a typical commercial airline crew flying 800-1000 hours per year, we estimate an annual exposure of 14.2 – 17.8 mSv of effective dose. For a corporate airline crew flying 100 – 400 hours per year and an average of 250 hours per year we estimate an annual exposure of 1.8 – 7.1 mSv (average of 4.5 mSv). Based on the current ICRP recommendations for radiation exposure for a nonpregnant radiation worker, the recommended exposure for a 5-year average is 20 mSv/yr. From this set of Raytheon flights, the airline crew would not be expected to exceed the ICRP recommendation for radiation exposure. However, as noted in Linborg and Nikjoo (2011), an annual exposure of 1 mSv is enough to invoke individual radiation monitoring, particularly in countries that have more stringent radiation standards.

245

246 **Table 1.** Mean and median ARMAS dose rates among all cruise altitude segments.

ARMAS Doses	Si Dose ($\mu\text{Gy/h}$)	Ti Dose ($\mu\text{Gy/h}$)	Dose Eq. ($\mu\text{Sv/h}$)	Ambient Dose ($\mu\text{Sv/h}$)	Effective Dose ($\mu\text{Sv/h}$)
Mean	2.8	4.1	8.5	13.1	17.7
Median	2.8	4.2	8.6	13.3	17.8

247

248

249 5.2 Comparisons of NAIRAS and ARMAS Dose Rates

250 The NAIRAS Run on Request (RoR) mode was run for each Raytheon flight in the database.

251 The NAIRAS model makes calculations of absorbed dose in silicon, absorbed dose in tissue,

252 ambient dose equivalent, dose equivalent, and effective dose. Assessing the model accuracy of

253 these dose rate calculations enables the utilization of NAIRAS for future aircraft flights and for

254 past flights where dosimeter measurements are not available. This will allow airline crews to

255 estimate radiation exposure over their careers as well as projected exposure on future flights.

256

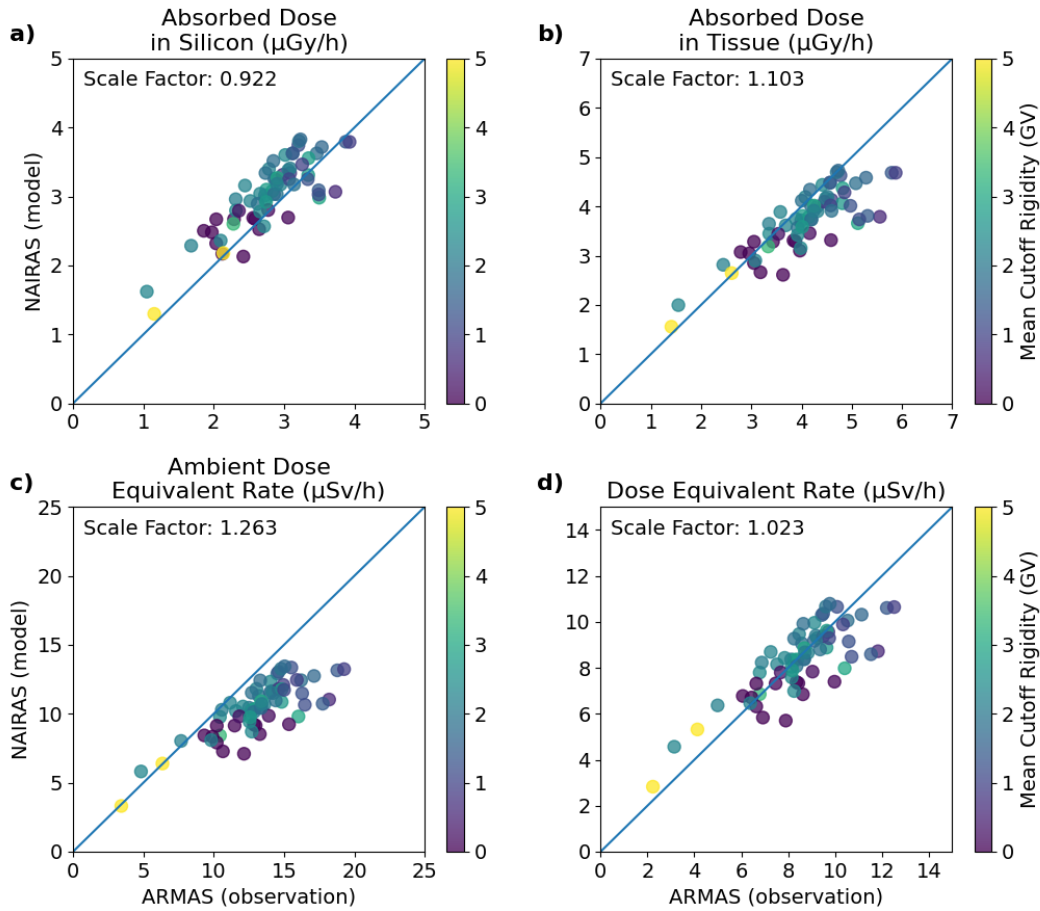
257 As stated above, the ARMAS dosimeter directly measures absorbed dose in silicon. While all

258 four NAIRAS calculated dose rates will be considered, we will focus on the evaluation of the

259 NAIRAS calculated absorbed dose in silicon since it is the fundamental quantity measured by the

260 ARMAS dosimeter. The correlation plot of absorbed dose rate in silicon shows very good

261 agreement between the model and observations (Figure 3a).



262
 263 **Figure 3.** Correlation plot of median (a) absorbed dose rate in silicon, (b) ambient dose
 264 equivalent rate, (c) dose equivalent rate, and (d) effective dose rate for all ARMAS and NAIRES
 265 cruise altitude segments.

266
 267 Quantitatively, NAIRES shows good agreement with the ARMAS dosimeter for absorbed dose
 268 in silicon, with a scale factor of 0.922. The percent difference in mean absorbed dose rate in
 269 silicon for all the cruise altitude segments reveals a difference of less than 24% for most of the
 270 flights (e.g., 59 out of 66 cruise altitude segments) which is notable because the ARMAS margin
 271 of error is $\sim 24\%$ (e.g., Tobiska et al., 2016).

272
 273 Correlation plots of the other three measured and modeled calculated doses reveal similar
 274 agreement (Figure 3b-d), with absorbed dose in tissue and dose equivalent rate also showing
 275 good agreement (e.g., scale factors of 1.103 and 1.023, respectively). The ambient dose
 276 equivalent rate shows a slight underprediction by NAIRES while the effective dose rate
 277 comparison shows a greater underprediction by NAIRES (scale factor of 1.494) because the
 278 ARMAS effective dose rate is derived based on model calculations from NAIRES version 2.0
 279 (not shown). As with the mean absorbed dose rate in silicon, we also find the percent difference
 280 in mean (and median) dose rates to be generally less than 24% for the dose equivalent and

281 ambient dose equivalent rates. A summary of the median and mean dose rates for ARMAS and
 282 NAIRAS and the percent differences are shown in Table 2. Considering all flight segments, the
 283 model calculated absorbed dose in silicon, tissue and the dose equivalent rate are in very good
 284 agreement with observations (less than 10% difference), while modeled ambient dose equivalent
 285 is within 21% of observations.

286

287 **Table 2.** Mean and median dose rates for NAIRAS and ARMAS from all cruise altitude
 288 segments.

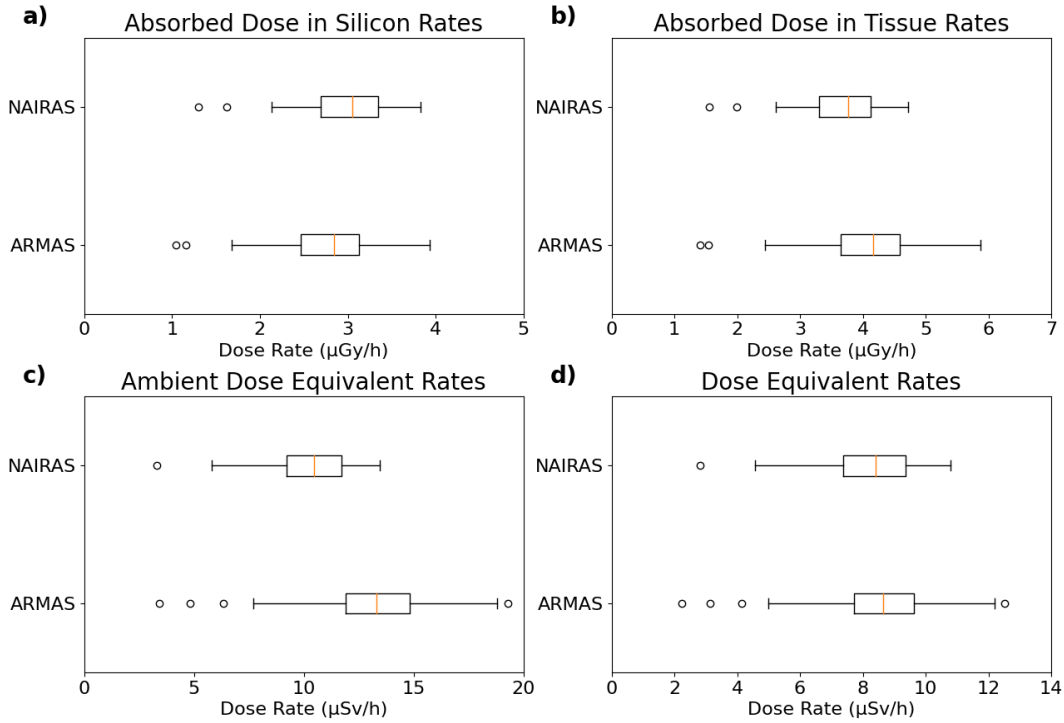
Mean Dose	Si Dose ($\mu\text{Gy/h}$)	Ti Dose ($\mu\text{Gy/h}$)	Dose Eq. ($\mu\text{Sv/h}$)	Ambient Dose ($\mu\text{Sv/h}$)	Effective Dose ($\mu\text{Sv/h}$)
ARMAS	2.8	4.1	8.5	13.1	17.7
NAIRAS	3.0	3.7	8.3	10.4	11.9
Difference (%)	8.27	-9.29	-2.35	-20.97	-33.05
Median Dose	Si Dose ($\mu\text{Gy/h}$)	Ti Dose ($\mu\text{Gy/h}$)	Dose Eq. ($\mu\text{Sv/h}$)	Ambient Dose ($\mu\text{Sv/h}$)	Effective Dose ($\mu\text{Sv/h}$)
ARMAS	2.8	4.2	8.6	13.3	17.8
NAIRAS	3.1	3.8	8.0	10.5	11.9
Difference (%)	7.39	-9.62	-6.94	-21.14	-32.85

289

290

291 To gain a better understanding of the distribution of dose rates measured by ARMAS and
 292 calculated by NAIRAS, boxplots of the dose rates for all cruise altitude segments are examined
 293 (Figure 4). For all flights, the interquartile range (IQR) for the absorbed dose rate in silicon is 2.5
 294 – 3.1 $\mu\text{Gy/h}$ in ARMAS and 2.7 – 3.3 $\mu\text{Gy/h}$ in NAIRAS. The absorbed dose rate in tissue IQR
 295 is 3.6 – 4.6 $\mu\text{Gy/h}$ in ARMAS and 3.3 – 4.1 $\mu\text{Gy/h}$ in NAIRAS. The ambient dose equivalent
 296 IQR is 11.9 – 14.8 $\mu\text{Sv/h}$ in ARMAS and 9.2 – 11.7 $\mu\text{Sv/h}$ in NAIRAS. The dose equivalent
 297 IQR is 7.7 – 9.6 $\mu\text{Sv/h}$ in ARMAS and 7.4 – 9.4 $\mu\text{Sv/h}$ in NAIRAS. And the effective dose rate
 298 IQR is 15.3 – 20.2 $\mu\text{Sv/h}$ in ARMAS and 10.5 – 13.4 $\mu\text{Sv/h}$ in NAIRAS. For the absorbed doses
 299 (e.g., silicon, tissue) and dose equivalent, there is good overlap between the modeled and
 300 observed IQR for the dose rates, particularly the absorbed dose rate in silicon. For ambient dose
 301 equivalent rate and effective dose, NAIRAS underestimates the dose rates, however, these are
 302 empirically derived dose quantities from ARMAS.

303



304
 305 **Figure 4.** Distributions of ARMAS measured and NAIRAS calculated dose rates for all flights
 306 and cutoff rigidities.

307
 308 Lastly, we summarize absorbed dose in silicon by cutoff rigidity. The majority of flights
 309 occurred in regions of low cutoff rigidity (0 – 4 GV). For flights in this radiation environment,
 310 the absorbed dose in silicon ranges from ~2.5 - 3.5 $\mu\text{Gy/h}$. Interestingly, the median dose rate is
 311 highest for flights in the 1 -2 GV range. However, this is likely due to the higher cruise altitudes
 312 at these lower latitude flights (compared to flights in the 0 – 1 GV range). For high cutoff rigidity
 313 environments (8 – 12 GV), the median dose rate is generally between 1.2 – 1.7 $\mu\text{Gy/h}$, well over
 314 1 $\mu\text{Gy/h}$ lower than flights in the 0 – 4 GV range (Table 3).

315
 316 **Table 3.** Median Si Dose Rate by Cutoff Rigidity ($\mu\text{Gy/h}$)

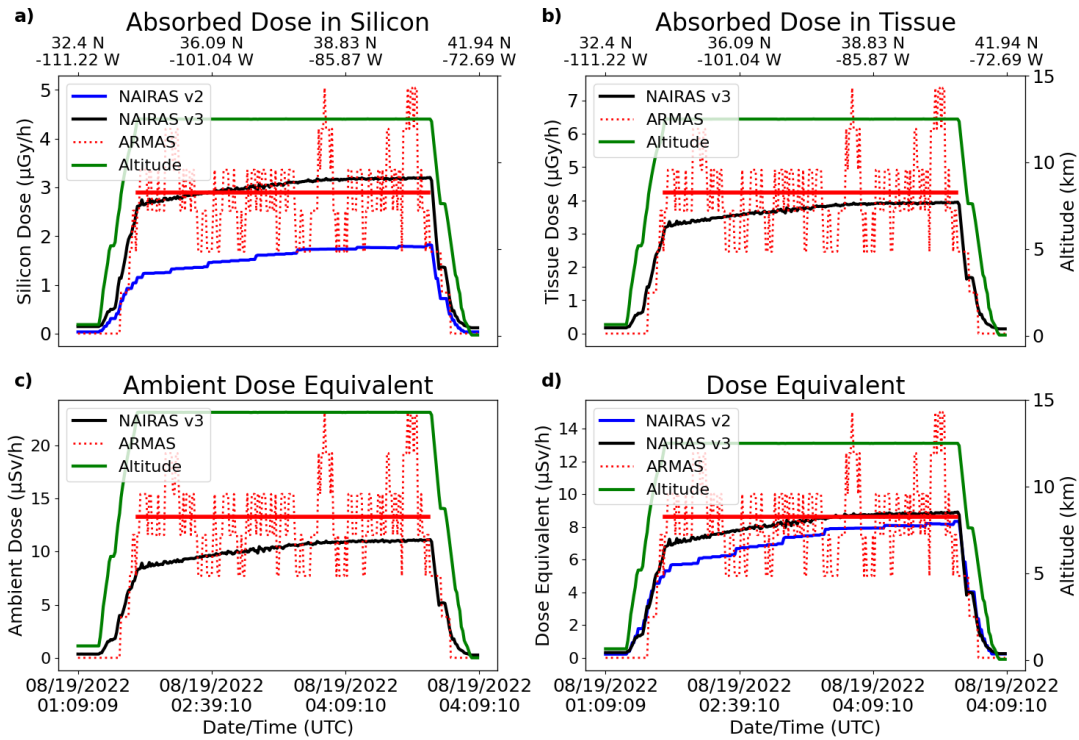
Cutoff Rigidity Range	NAIRAS	ARMAS	Number of Qualifying Trajectory Points
0 – 1 GV	2.7	2.5	2206
1 – 2 GV	3.5	3.4	2486
2 – 3 GV	3.1	2.5	1840
3 – 4 GV	2.9	2.5	333
4 – 5 GV	2.7	2.5	44
5 – 6 GV	2.4	2.5	33
6 – 7 GV	2.2	1.7	9
7 – 8 GV	1.9	2.5	9
8 – 9 GV	1.7	1.7	17

9 – 10 GV	1.5	1.7	33
10 – 11 GV	1.4	1.7	44
11 – 12 GV	1.3	0.8	30

317
318
319
320
321
322
323

5.3 Case Study 1: Domestic Flight from San Jose, CA to Hartford, CT

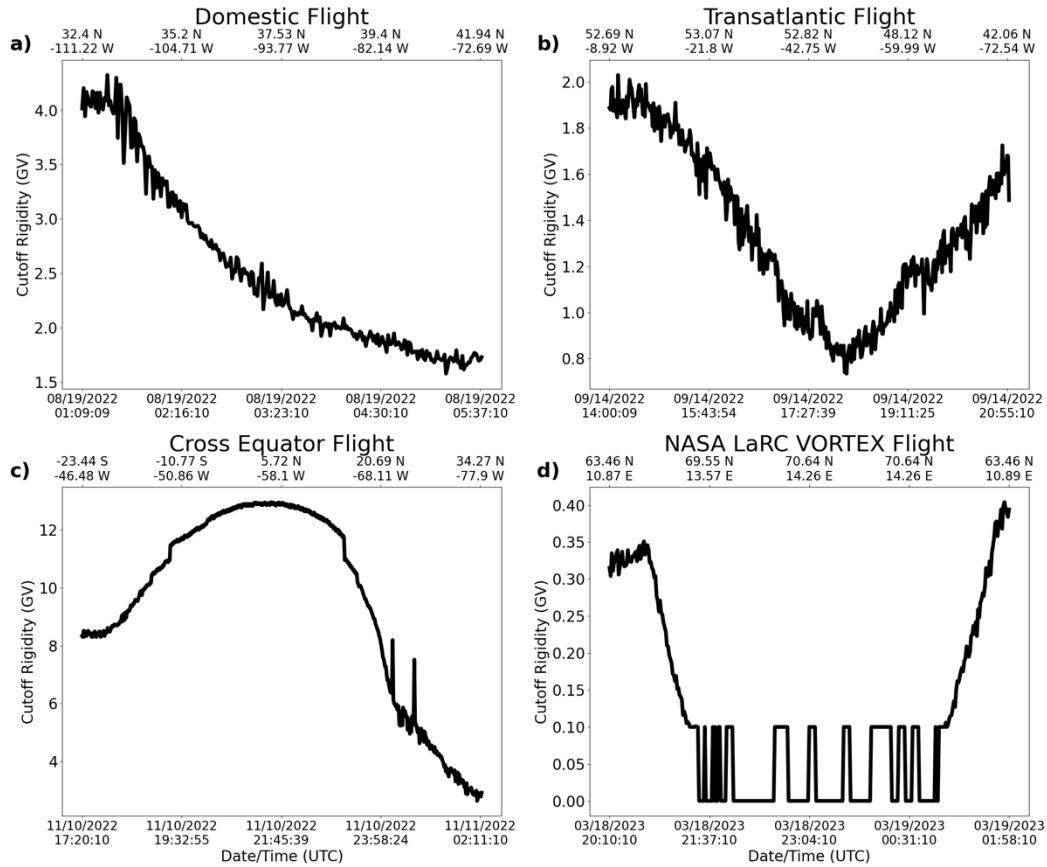
To illustrate the dose rates over a typical cross-country domestic flight, timeseries plots of the four dose rates are shown for a flight from Tucson, AZ to Hartford, CT (Figure 5). This flight is characterized by a mean cruise altitude of 12.5 km and mean latitude of 37.88° N.



324
325
326
327
328
329
330
331
332
333
334
335
336
337
338
339

Figure 5. Timeseries plots of (a) absorbed dose rate in silicon, (b) absorbed dose rate in tissue, (c) ambient dose equivalent, and (d) dose equivalent for the August 19, 2022 01:09 UTC flight from Tucson, AZ to Hartford, CT. The green line shows aircraft altitude (right axis), the red line shows the ARMAS dose rate (left axis), the red dashed line shows the mean ARMAS dose rate at cruise altitude (left axis), and the black line shows the NAIIRAS dose rate (left axis).

The cutoff rigidity for this flight ranges from 1.4 GV to 3.5 GV (Figure 6a). Overall, there is very good agreement between NAIIRAS and the ARMAS dosimeter. At cruise altitude, the mean absorbed dose in silicon is 2.9 and 3.0 μGy/h in ARMAS and NAIIRAS, respectively, a 4.14% difference. As in Figure 6a, the cutoff rigidity is 4.1 GV at the beginning of the flight and decreases to ~1.7 GV. The NAIIRAS and the ARMAS dose rates show a slight increase in the dose rate over the duration of the flight, reflecting this change in cutoff rigidity, while the cruise altitude remains constant. Compared to NAIIRAS version 2.0, the latest updates to NAIIRAS produce higher dose rates for all modeled dose quantities and are in much better agreement with the dosimeter.

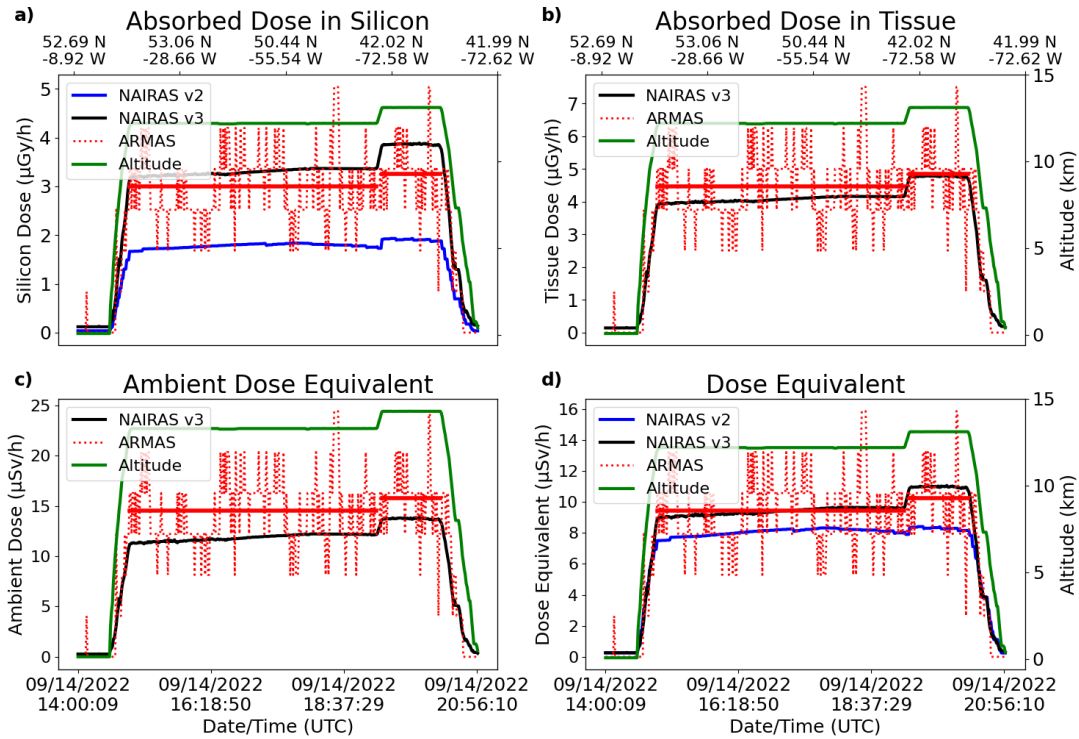


341
 342 **Figure 6.** Timeseries of cutoff rigidity (GV) for (a) a typical United States domestic flight from
 343 Tucson, AZ to Hartford, CT, (b) a transatlantic flight from Shannon, Ireland to Hartford, CT,
 344 USA, (c) a cross-equator flight from São Paulo, Brazil to Wilmington, NC, USA, and (d) a high
 345 latitude flight in Norway.

346
 347 **5.4 Case Study 2: Transatlantic Flight from Shannon, Ireland to Hartford, CT, USA**

348 To illustrate typical dose rates for an international flight, particularly one that approaches a
 349 cutoff rigidity of 0 GV (Fig. 6b), timeseries of dose rates and cutoff rigidity are shown from a
 350 flight from Shannon, Ireland to Hartford, CT, USA. This flight had cruise altitude segments of
 351 12.19 km (mean latitude of 52.49° N) and 12.89 km (mean latitude of 46.75° N). For the two
 352 cruise altitude segments, the mean ARMAS measured absorbed dose rate in silicon is 3.0 and 3.2
 353 $\mu\text{Gy/h}$ and the mean NAIRAS calculated absorbed dose rate in silicon is 3.3 and 3.7 $\mu\text{Gy/h}$ (Fig.
 354 7). For the two cruise altitude segments, the percent difference in mean absorbed dose rate in
 355 silicon is 10.04% and 16.84%, both within the margin of error of the ARMAS dosimeter.
 356 Interestingly, the highest dose rate does not occur during the minima in cutoff rigidity, but rather
 357 the highest cruise altitude, demonstrating that GCR dose rate has a higher dependence on altitude
 358 than cutoff rigidity. This result is consistent with Tobiska et al. (2016) who showed that the dose
 359 rate doubles for every 2 km increase in altitude. As in the domestic flight, the NAIRAS version

360 3.0 dose rates are all higher than in version 2.0 and are generally in better agreement with
 361 ARMAS.
 362

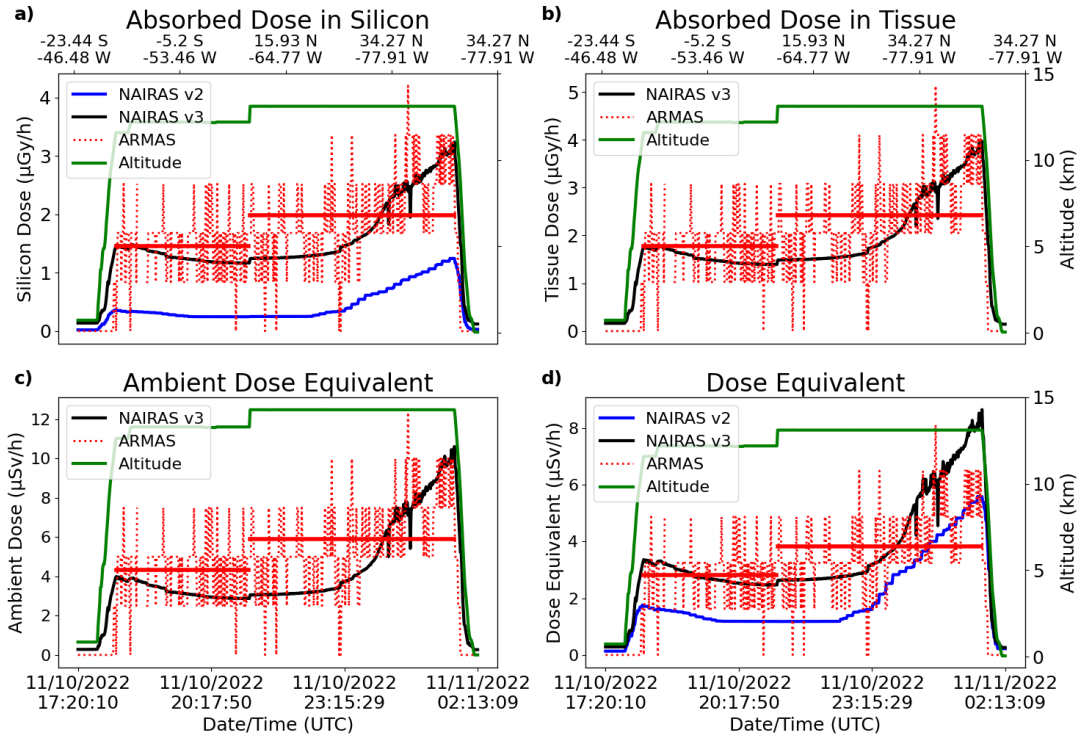


363
 364 **Figure 7.** As in Figure 5, but for the transatlantic flight from Shannon, Ireland to Hartford, CT,
 365 USA.
 366

367 **5.5 Case Study 3: Cross-Equator Flight from São Paulo, Brazil to Wilmington, NC, USA**

368 One flight in this dataset crossed the equator. As such, it represents a demonstration of dose rates
 369 at low latitudes and high cutoff rigidities. The flight departed from São Paulo, Brazil at a
 370 relatively low latitude (23.44°S) and high cutoff rigidity (~8 GV) before crossing the equator and
 371 reaching the highest cutoff rigidity for any flight in this dataset (~13 GV). As the flight continues
 372 to the north towards the northern hemisphere mid-latitudes, the cutoff rigidity rapidly decreases
 373 (Fig. 6c), and dose rates increase (beginning 11/10/2022 ~23:00 UT).
 374

375 For the two cruise altitude segments (12.23 km, 13.11 km), the mean absorbed dose in silicon is
 376 1.2 and 2.1 μGy/h in ARMAS, respectively, and 1.3 and 2.2 μGy/h in NAIAS, respectively
 377 (Fig. 8). The percent differences for these two cruise altitude segments are 12.43% and 1.98%,
 378 both well within the ARMAS margin of error. Compared to the international and domestic
 379 flights, which were both in the northern hemisphere mid-latitudes, the average dose rate for this
 380 flight is about 50% lower. Similar to the previous two flights, NAIAS version 3.0 shows much
 381 better agreement than NAIAS version 2.0 (NAIRAS version 2.0 absorbed dose in silicon was
 382 70% lower than ARMAS, NAIAS version 3.0 only 5% lower than ARMAS).
 383

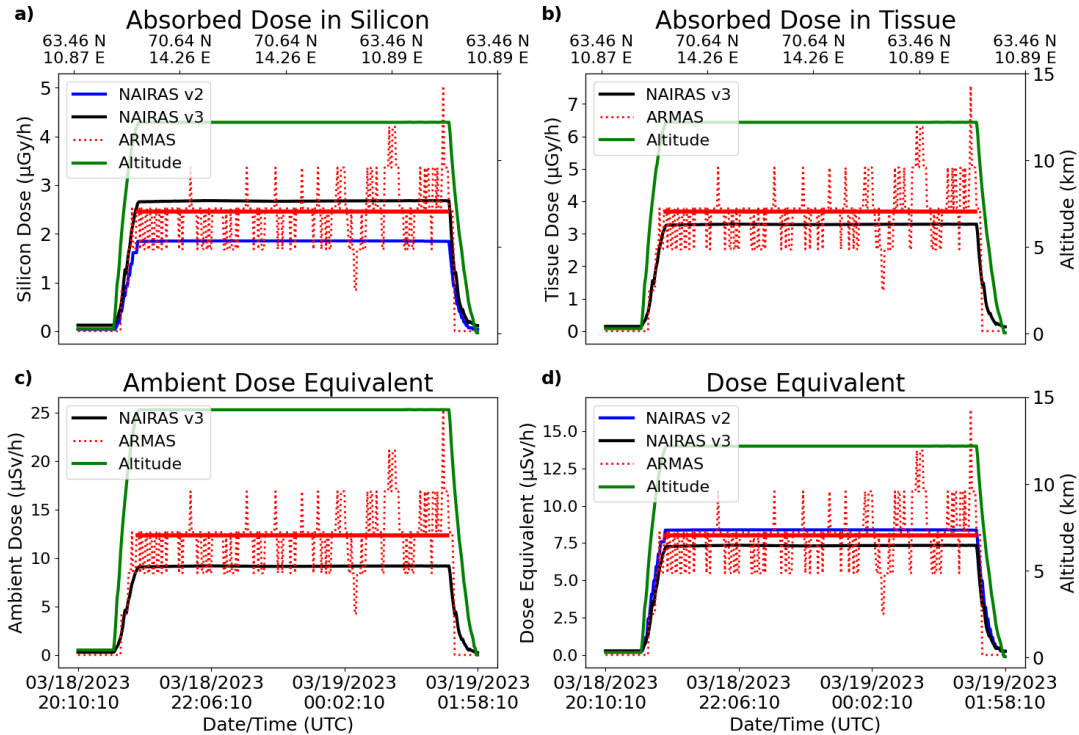


384
 385 **Figure 8.** As in Figure 5, but for a cross-equatorial flight from São Paulo, Brazil to Wilmington,
 386 NC, USA.

387

388 **5.6 Case Study: NASA Langley Research Flight in Norway**

389 Several high-latitude flights took place in March 2023 with the ARMAS dosimeter as part of a
 390 NASA LaRC Vorticity Experiment (VortEx) Norway Sounding Rocket Mission. In contrast to
 391 the Raytheon corporate flights, these were research flights designed to study large vortices in the
 392 upper atmosphere. These flights provide an interesting contribution to the dataset due to the low
 393 cutoff rigidity (near 0 GV for the duration of the flight (Fig. 6d)), which represents a typical
 394 high-end for radiation dose exposure. For these flights, the NAIAS-calculated dose rates agree
 395 quite well with the ARMAS measurements (Figure 9). For the flight shown in Figure 9, the mean
 396 dose rate in silicon is 2.5 $\mu\text{Gy/h}$ and 2.7 $\mu\text{Gy/h}$ from ARMAS and NAIAS, respectively, with a
 397 mean percent difference of 8.9%. The mean latitude for this flight is 69.8°N and the mean cutoff
 398 rigidity is 0.05 GV (Fig. 6d). Unlike the other flights discussed above, there is little difference
 399 between the NAIAS version 2.0 and version 3.0 dose rates, with the exception of the absorbed
 400 dose rate in silicon. Overall, NAIAS version 3.0 is an improvement over NAIAS version 2.0.



401
 402 **Figure 9.** As in Figure 5, but for a NASA LaRC research flight in Norway (Trondheim Airport,
 403 Værnes).
 404

405 5.7 Improvements over NAIRAS version 2.0

406 The main improvements in NAIRAS version 3.0 are the extension of the atmosphere to free-
 407 space and inclusion of multi-directional ray transport, improvements to the SEP proton spectral
 408 fitting algorithm, and the inclusion of GCR ultra-heavy ions. The multi-directional transport
 409 improves the absorbed dose quantities (e.g., absorbed dose in silicon, tissue) which are sensitive
 410 to the charged particle environment. Additionally, the expansion of the GCR ultra-heavy ions
 411 from nickel ($Z = 28$, $A = 58$) to uranium ($Z = 92$, $A = 238$) increases the maximum LET from
 412 $31.9 \text{ MeV-cm}^2/\text{mg}$ to $110.2 \text{ MeV-cm}^2/\text{mg}$ (Mertens et al., 2023a). This update to NAIRAS
 413 version 3.0 also increases the dose rates at aircraft cruise altitudes. Together these updates have
 414 yielded an increase especially in absorbed dose rate calculations, bringing the model in much
 415 better agreement with the dosimeter measurements. For calculations of absorbed dose in silicon
 416 among the four flights discussed in detail in Sections 5c-f, NAIRAS version 3.0 dose rates are
 417 both higher than NAIRAS version 2.0 and in better agreement with the ARMAS dosimeter. In
 418 general, differences in absorbed dose rates between NAIRAS version 2.0 and ARMAS are 30%
 419 greater for the cruise altitude segments in this study, compared to NAIRAS version 3.0 and
 420 ARMAS percent differences.
 421

422 6 Summary and Future Work

423 Dose rate measurements from the ARMAS FM dosimeter on board 39 Raytheon corporate and 6
 424 NASA LaRC research flights provide a good range in expected dose rates for airline crews.
 425 Considering all flights, the ARMAS derived median effective dose rate of $17.8 \text{ } \mu\text{Sv/h}$, which
 426 yields an annual dose exposure of 17.8 mSv for a flight crew flying 1000 hours per year. For a
 427 corporate airline crew flying 400 hours per year, it is estimated that the crew would be exposed

428 to a total of 7.1 mSv. However, based on comparisons with the NAIRAS model, it is likely that
429 the ARMAS derived effective dose rate should be reevaluated with NAIRAS version 3.0
430 calculations. Based on the NAIRAS modeled effective dose rate, a 1000-hour commercial flight
431 crew is only exposed to 11.9 mSv over a typical 1000-hour year, much lower than the ARMAS
432 estimate as well as the ICRP recommendation.

433
434 Considering the dose rates for absorbed dose in silicon, dose equivalent, and ambient dose
435 equivalent, there is very good agreement between NAIRAS and ARMAS. Overall, for the
436 majority of cruise altitude segments, the mean (and median) dose rates are within the ARMAS
437 uncertainty of 24%. This result provides confidence in using the NAIRAS model for making
438 dose exposure estimates for flight trajectories. Furthermore, comparing dose rate estimates from
439 NAIRAS version 2.0 to NAIRAS version 3.0 shows substantial improvements in the modeled
440 dose rate calculations.

441
442 While this dataset provides a fairly representative sample of corporate aircraft flight paths, the
443 majority of flights occurred over northern hemisphere midlatitudes, particularly in the United
444 States. For a more thorough evaluation, a wider range of flights should be considered. Currently,
445 there is an ongoing effort to evaluate the larger collection of flights (over 1000 flights) using the
446 ARMAS FM dosimeter occurring between 2013 and 2023. This dataset consists of flights
447 ranging from 8 km – 550 km in altitude and includes NASA, commercial and corporate flights,
448 as well as high altitude balloons, commercial suborbital, and the International Space Station
449 (ISS). This evaluation is expected to yield a broader understanding of the expected dose rates as
450 well as a more robust comparison with NAIRAS version 3.0.

451 452 **Acknowledgements**

453 The NAIRAS model extension from the atmosphere to space was funded by the NASA
454 Engineering and Safety Center (NESC) assessment TI-19-01468. The improvements in SEP
455 event spectral fitting and cutoff rigidity modeling were funded by the NASA Science Mission
456 Directorate, Heliophysics Division, Space Weather Science Applications Program.

457 458 **Data Availability Statement**

459 The NAIRAS RoR service is available at CCMC (Zheng, 2023). Descriptions of the NAIRAS
460 model are given by Mertens et al. (2010, 2012, and 2013). The ARMAS database can be
461 accessed at
462 [https://sol.spacenvironment.net/ARMAS_Archive/ARMAS_dirIP_Report_UUID_YMDhms_L1](https://sol.spacenvironment.net/ARMAS_Archive/ARMAS_dirIP_Report_UUID_YMDhms_L1_L4_data_txts/)
463 [L4_data_txts/](https://sol.spacenvironment.net/ARMAS_Archive/ARMAS_dirIP_Report_UUID_YMDhms_L1_L4_data_txts/)

464
465
466
467
468
469
470
471
472
473

474
475
476
477
478
479
480
481
482
483
484
485
486
487
488
489
490
491
492
493
494
495
496
497
498
499
500
501
502
503
504
505
506
507
508
509
510
511
512
513
514
515
516
517
518
519

References

- American Meteorological Society (2007), Integrating space weather observation and forecasts into aviation operations. Technical Report, American Meteorological Society Policy Program & SolarMetrics, Washington, D. C.
- Bennett, L. G. I., Lewis, B. J., Bennett, B. H., McCall, M. J., Bean, M., Doré, L., and Getley, I. L. (2013), A survey of the cosmic radiation exposure of Air Canada pilots during maximum galactic radiation conditions in 2009. *Radiat. Meas.*, *49*, 103 – 108.
- Copeland, K, Sauer, H. H., Duke, F. E., and Friedberg, W. (2008), Cosmic radiation exposure on aircraft occupants on simulated high-latitude flights during solar proton events from 1 January 1986 through 1 January 2008. *Adv. Space Res.*, *42*, 1008 – 1029.
- Copeland, K., Friedberg, W., Sato, T., and Niita, K. (2012), Comparison of fluence-to-dose conversion coefficients for deuterons, tritons, and helions, *Radiation Protection Dosimetry*, *148*(3), 344 – 351. <https://doi.org/10.1093/rpd/ncr035>.
- Copeland, K. (2017), CARI-7A: Development and validation. *Radiation Protection Dosimetry*, *178*(4), 419 – 431. <https://doi.org/10.1093/rpd/ncw369>.
- Dyer, C., Hands, A., Lei, F., Truscott, P., Ryden, K. A., Morris, P., Getley, I., Bennett, L., Bennett, B., and Lewis, B. (2009), Advances in measuring and modeling the atmospheric radiation environment, *IEEE Trans. Nucl. Sci.*, *56*(8), 3415 – 3422.
- Gopalswamy, N., Yashiro, S., Lara, A., Kaiser, M. L., Thompson, B. J., Gallagher, P. T., and Howard, R. A. (2003), Large solar energetic particle events of solar cycle 23: A global view. *Geophys. Res. Lett.*, *30*(12), 8015. <https://doi.org/10.1029/2002GL016435>.
- ICRP (2007), ICRP Publication 103: The 2007 Recommendations of the International Commission on Radiological Protection, *37*(2-4), Elsevier, Oxford.
- IEC (2006), Process management for avionics—Atmospheric radiation effects—Part 1: Accommodation of atmospheric radiation effects via single event effects within avionics electronic equipment. IEC/TS 62396-1:2006(E), International Electrotechnical Commission.
- Lindborg, L., and Nikjoo, H. (2011), Microdosimetry and radiation quality determinations in radiation protection and radiation therapy. *Radiat. Prot. Dosim.*, *143*(2-4), 402 – 408.
- Matthiä, D., Berger, T., Mrigakshi, A. I., and Reitz, G. (2013), A ready-to-use galactic cosmic ray model. *Advances in Space Research*, *51*(3), 329-338.

- 520 <https://doi.org/10.1016/j.asr.2012.09.022>.
- 521
- 522 Matthiä, D., Meier, M. M., and Reitz, G. (2014), Numerical calculation of the radiation exposure
523 from galactic cosmic rays at aviation altitudes with the PANDOCA core model. *Space*
524 *Weather*, *12*, 161-171. <https://doi.org/10.1002/2013SW001022>.
- 525
- 526 Meier, M. M., Trompier, F., Ambrozova, I., Kubancak, J., Matthiä, D., Ploc, O., et al. (2016),
527 CONCORD: Comparison of cosmic radiation detectors in the radiation field at aviation
528 altitudes, *Journal of Space Weather and Space Climate*, *6*.
529 <https://doi.org/10.1051/swsc/2016017>.
- 530
- 531 Meier, M. M., Copeland, K., Matthiä, D., Mertens, C. J., and Schennetten, K. (2018), First steps
532 toward the verification of models for the assessment of the radiation exposure at aviation
533 altitudes during quiet space weather conditions. *Space Weather*, *16*, 1269-1276,
534 <https://doi.org/10.1029/2018SW001984>.
- 535
- 536 Mertens, C. J., Kress, B. T., Wiltberger, M., Blattnig, S. R., Slaba, T. S., Solomon, S. C., and
537 Engel, M. (2010), Geomagnetic influence on aircraft radiation exposure during a solar
538 energetic particle event in October 2003. *Space Weather*, *8*, S03006,
539 <https://doi.org/10.1029/2009SW000487>.
- 540
- 541 Mertens, C. J., Kress, B. T., Wiltberger, M., Tobiska, W. K., Grajewski, B., and
542 Xu, X. (2012), Atmospheric ionizing radiation from galactic and solar cosmic rays,
543 in *Current Topics in Ionizing Radiation Research*, edited by M. Nenoï, InTech Publisher,
544 (ISBN 978-953-51-0196-3).
- 545
- 546 Mertens, C. J., Meier, M. M., Brown, S., Norman, R. B., and Xu, X. (2013). NAIRAS aircraft
547 radiation model development, dose climatology, and initial validation. *Space Weather*,
548 *11*(10), 603-635, <https://doi.org/10.1002/swe.20100>.
- 549
- 550 Mertens, C. J., Gronoff, G. P., Phoenix, D., Zheng, Y., Petrenko, M., Buhler, J., Jun, I., Minow,
551 J., and Willis, E. (2023a), NAIRAS Ionizing Radiation Model: Extension from
552 Atmosphere to Space. Technical Publication, NASA Langley Research Center, Hampton,
553 VA.
- 554
- 555 Mertens, C. J., Gronoff, G. P., Zheng, Y., Petrenko, M., Buhler, J., Phoenix, D., Willis, E., Jun,
556 I.,
557 Minow, J. (2023b), NAIRAS Model Run-On-Request Service at CCMC. *Space Weather*,
558 *21*(5), <https://doi.org/10.1029/2023SW003473>.
- 559
- 560 Mertens, C. J., Gronoff, G. P., Zheng, Y., Buhler, J., Willis, E., Petrenko, M., Phoenix, D., Jun,
561 I.,
562 and Minow, J. (2023c), NAIRAS Atmospheric and Space Radiation Environment Model.
563 *IEEE Transactions on Nuclear Science*, <https://doi.org/10.1109/TNS.2023.3330675>.
- 564
- 565 Tobiska, W. K., et al. (2016), Global real-time dose measurements using the Automated

566 Radiation Measurements for Aerospace Safety (ARMAS) system. *Space Weather*, 14,
567 1053–1080, <https://doi.org/10.1002/2016SW001419>.

568

569 Tysganenko, N. A. (1989), Determination of magnetic current system parameters and
570 development of experimental geomagnetic field models based on data from IMP and
571 HEOS satellite. *Planetary and Space Science*, 37, 5 – 20.

572

573 Tysganenko, N. A. and Sitnov, N. I. (2005), Modeling the dynamics of the inner magnetosphere
574 during strong geomagnetic storms. *J. Geophys. Res.*, 110, A03208,
575 <https://doi.org/10.1029/2004JA010798>.

576

577 Zheng, Y. (2023). User interface to NAIRAS model (Version 3.0) run-on-request service.
578 [Software]. <https://ccmc.gsfc.nasa.gov/models/NAIRAS~3.0>